

Scaling Self-Supervised End-to-End Driving with Multi-View Attention Learning

Yi Xiao

Computer Vision Center (CVC)
Campus UAB, Barcelona, Spain

yxiao@cvc.uab.cat

Diego Porres Bustamante

Computer Vision Center (CVC)
Campus UAB, Barcelona, Spain

dporres@cvc.uab.cat

Felipe Codevilla

Montreal Institute for Learning Algorithms (MILA)
Montreal, Canada

felipe.alcm@gmail.com

Antonio M. López

Computer Vision Center (CVC)
Campus UAB, Barcelona, Spain

antonio@cvc.uab.cat

Abstract

On end-to-end driving, a large amount of expert driving demonstrations is used to train an agent that mimics the expert by predicting its control actions. This process is self-supervised on vehicle signals (e.g., steering angle, acceleration) and does not require extra costly supervision (human labeling). Yet, the improvement of existing self-supervised end-to-end driving models has mostly given room to modular end-to-end models where labeling data intensive format such as semantic segmentation are required during training time. However, we argue that the latest self-supervised end-to-end models were developed in sub-optimal conditions with low-resolution images and no attention mechanisms. Further, those models are confined with limited field of view and far from the human visual cognition which can quickly attend far-apart scene features, a trait that provides an useful inductive bias. In this context, we present a new end-to-end model, trained by self-supervised imitation learning, leveraging a large field of view and a self-attention mechanism. These settings are more contributing to the agent's understanding of the driving scene, which brings a better imitation of human drivers. With only self-supervised training data, our model yields almost expert performance in CARLA's Nocrash metrics and could be rival to the SOTA models requiring large amounts of human labeled data. To facilitate further research, our code will be released.

1. Introduction

End-to-end autonomous driving (EtE-AD) relies on deep models trained to mimic human drivers (experts) [27]. Broadly, we can classify them according to their training strategy. Some models are self-supervised on vehicle signals (e.g., steering angle, acceleration) while others require

additional supervision (e.g., semantic segmentation, bounding boxes, privileged information). A major drawback of the latter is the curse of human-based sensor data labeling, i.e., as for traditional AD pipelines [14,33]. In contrast, self-supervised EtE-AD models can be trained on vehicle signals from the million daily miles of available human driving data, i.e., not requiring human-based sensor data labeling. This paper focuses on self-supervised EtE-AD.

Despite the appealing idea of developing self-supervised EtE-AD models, their progress has mostly stalled, giving space to EtE-AD models supervised by a significantly large amount of labeled sensor data [5–7, 16, 19, 20, 23, 25, 31, 34], or by privileged information from the the driving environment as required by reinforcement learning [29, 34]. This situation may be due to the apparent lack of scalability of self-supervised EtE-AD models raised in a few works [10, 26], including [9], where the representative self-supervised model known as CILRS is proposed. However, CILRS was developed in suboptimal conditions: limited driving episodes based on a single and rather deterministic expert driver, very low resolution images depicting a relatively narrow horizontal field of view (on-board images roughly display a single lane), and without applying any attention mechanism. Overall, this drives to a poor performance in newer benchmarks, which, eventually, can mislead non-expert readers and new practitioners in the field regarding the potential of self-supervised EtE-AD.

Accordingly, we present *CIL++*, a strong EtE-AD model trained by self-supervised conditional imitation learning, i.e., as CILRS. We improve on CILRS key limitations, rising the performance of *CIL++* to be on par with top-performing supervised methods. First, we drastically increase the field of view by using a horizontal field of view (HFOV) similar to human drivers, which runs on $180^\circ - 220^\circ$. Further, we propose a visual transformer architec-

ture [30] which acts as a mid-level attention mechanism for these views allowing CIL++ to associate feature map patches (tokens) across different views. CIL++ performs at expert level the CARLA *NoCrash* metrics. Moreover, CIL++ is the first self-supervised EtE-AD model capable of obtaining competitive results on complex CARLA’s towns.

2. Related Work

Learning a driving policy from experts, instead of handcrafting it, is a really appealing idea. Accordingly, EtE-AD, where a deep model is trained by imitation learning, has become an active research topic [27]. Pioneering works following this approach are [3, 4, 18, 22]. However, it was the public release of the CARLA simulator [13], together with a vision-based EtE-AD model trained and tested on CARLA [8], what attracted great attention to this paradigm [2, 5–7, 9, 16, 19, 20, 23, 25, 28, 31, 32, 34].

Basically, we can find two ways of approaching EtE-AD according to the output of the underlying deep model. On the one hand, different proposals output waypoints on bird-eye-view (BeV) coordinates [2, 5–7, 20, 23, 25]. These are then used by a controller for providing the proper steering and acceleration in driving. Note that generating BeVs involves 3D knowledge of the scene. On the other hand, other proposals directly output the ego-vehicle signals (steering, acceleration) [8, 9, 16, 19, 21, 28, 32, 34], which act on the vehicle either directly or after some signal-stabilizer filtering (*e.g.*, using a PID). Both approaches have been combined, *e.g.*, in [31], where a branch of the EtE-AD model is used to predict waypoints and another to predict ego-vehicle signals, being the model output a combination of both, weighted according to the perceived road curvature.

Another important difference among EtE-AD models is the type of required supervision for their training. For instance, some models require semantic segmentation labels at training time [2, 6, 7, 16], sometimes together with object bounding boxes (BBs) [23], or BBs and HD maps [2]. Other models are only self-supervised on ego-vehicle available signals [3, 4, 8, 9, 18, 22], thus no human-labeled sensor data required. EtE-AD models can also fuse multi-modal sensor data such as RGB image and depth from either LiDAR [5, 23, 25] or monocular depth estimation [32].

Overall, recent literature presents results where pioneering self-supervised EtE-AD models such as CILRS [8] are clearly outperformed by those using additional supervision (semantic segmentation, object BBs, *etc.*). This is to be expected since, for instance, the currently top-performing EtE-AD model, termed as MILE [16], relies on a training procedure requiring $\approx 3M$ of images labeled for semantic segmentation. Another top-performing EtE-AD model, NEAT [7], requires $\approx 130K$ of those. In addition, Roach [34] leverages the teacher/student mechanism. First, a *teacher* model (Roach RL) is trained using environment-

privileged information and reinforcement learning. Then, it supervises the training of a *student* model (Roach IL) by applying imitation learning. In this paper, we call the student model as RIM.

Moreover, CILRS was developed under completely different conditions than we have today: only using single-lane towns in CARLA simulator (Town01 and Town02), using very low-resolution images depicting a narrow horizontal field of view (roughly, one-lane-width views), without including any attention mechanism, and relying on the default CARLA’s expert driver, which is handcrafted. Overall, this drives it to a poor performance on newer benchmarks.

Our model, CIL++, is a direct successor of CILRS, aiming at bringing back the competitiveness of self-supervised EtE-AD. In particular, for training and testing CIL++, we use the multi-town setting available in the latest version of CARLA (0.9.13). Moreover, as in recent works [16], to collect training data (images and ego-vehicle signals), we use an expert [34] with better driving performance than the CARLA’s default one. In addition, we use a wider horizontal field of view (HFOV=180°), in the range of human drivers. This kind of inductive bias is crucial to avoid injecting undesired causal confusion when training the model. For instance, while collecting driving episodes for training, the ego-vehicle may be stopped at a red traffic light because the expert driver has access to the privileged information of the environment. However, this red light may not even be captured by the onboard camera due to a narrow HFOV. This was observed in CILRS which was using HFOV=100°. In fact, using wide HFOVs has become a common practice to develop EtE-AD models (*e.g.*, [7, 16, 23, 25, 34]). As we would do in the real world to avoid image distortion, we use three forward-facing cameras with HFOV=60° each and without view overlapping. Finally, in order to jointly consider the image content from the three cameras (views), we propose a visual transformer [30] which acts as a mid-level attention mechanism for these views. All these improvements over CILRS make CIL++ competitive.

On the other hand, as CILRS, we use the current ego-vehicle speed and high-level navigation commands as input signals to the model. However, unlike CILRS, we also consider left/right lane changes as possible command values at testing time. Note that some supervised methods such as MILE, instead of processing a high-level navigation command, use as input the road shape pattern to be expected according to the current position of the ego-vehicle. Given a curve, this pattern can be more or less curved according to the corresponding lane curvature. In CILRS and CIL++, high-level commands (*e.g.*, *continue* in this lane) are equivalent to those from a navigation system for global planning. In fact, such navigation commands together with the ego-vehicle speed are the only information that CIL++ uses beyond the multi-view images. This is in contrast with other

supervised models such as NEAT [7], which use explicit traffic light detection at testing time.

As we will see, even CIL++ is not using supervision at all, it outperforms RIM and is quite on par with MILE.

3. Building CIL++: Self-Supervised EtE-AD with Multi-view Attention Learning

3.1. Problem Setup

CIL++ is trained by self-supervised imitation learning, which we formalize as follows. Expert demonstrators (drivers) produce an action \mathbf{a}_i (ego-vehicle maneuver) when encountering an observation \mathcal{O}_i , (sensor data, signals) given the expert policy $\pi^*(\mathcal{O}_i)$ (driving skills, attitude, *etc.*). The basic idea behind imitation learning is to train an agent (here CIL++) that mimics an expert by using these observations.

Prior to training an agent, we need to collect a dataset comprised of observation/action pairs $\mathcal{D} = \{(\mathbf{o}_i, \mathbf{a}_i)\}_{i=1}^N$ generated by the expert. This dataset is in turn used to train a policy $\pi_\theta(\mathbf{o}_i)$ which approximates the expert policy. The general imitation learning objective is then

$$\operatorname{argmin}_\theta \mathbb{E}_{(\mathbf{o}_i, \mathbf{a}_i) \sim \mathcal{D}} [\mathcal{L}(\pi_\theta(\mathbf{o}_i), \mathbf{a}_i)] . \quad (1)$$

During testing time, we assume that only the trained policy $\pi_\theta(\mathbf{o}_i)$ will be used and no expert will be available.

3.2. Architecture

Fig.1 shows an overview of CIL++’s architecture. Our model is mainly comprised of three parts: state embedding, transformer encoder, and action prediction module, which we describe in the following.

3.2.1 State Embedding

At time t , the current state \mathcal{X}_t consists of a set of images from the left, central, and right cameras $\mathbf{X}_t = \{\mathbf{x}_{l,t}, \mathbf{x}_{c,t}, \mathbf{x}_{r,t}\}$, the ego-vehicle’s forward speed $s_t \in \mathbb{R}$, and a high-level navigation command $\mathbf{c}_t \in \mathbb{R}^k$ which is encoded as a one-hot vector.

As discussed in [12], the lack of inductive biases makes transformer models require more data to achieve good performance. In order to possess the inherent properties of CNNs (*i.e.*, exploiting locality and translation equivariance), as well as leveraging the attention mechanism of transformers, we propose to adapt the hybrid mode suggested in [12] to our case. At time t , each image $\mathbf{x}_{v,t} \in \mathbb{R}^{W \times H \times 3}$ from the multi-view camera setting is processed by a share-weight ResNet34 [15], pre-trained on ImageNet [11]. Then, for each view v , we take the resulting feature map $\mathbf{f}_{v,t} \in \mathbb{R}^{w \times h \times c}$ from the last convolutional layer of ResNet34, where $w \times h$ is the spatial size and c indicates the feature dimension. Each feature map is then flattened

along the spatial dimensions, resulting in $P \times c$ tokens, where $P = w * h$ is the number of spatial features per image. Since we will set our cameras to a resolution of $W \times H = 300 \times 300$ pixels, for each one we obtain $P = 100$ patches with $c = 512$ from the ResNet34 backbone.

Since we use $|\mathbf{X}_t| = 3$ views (cameras), we take the flattened patches for each view, and tokenize them as the whole sequence with length $S = |\mathbf{X}_t| * w * h$ for further feeding into the transformer model. To provide the positional information for each token, we apply the standard learnable 1D positional embedding $\mathbf{p} \in \mathbb{R}^{S \times c}$ as done in [12], which is added directly to the token.

The forward speed s_t and command \mathbf{c}_t are linearly projected to \mathbb{R}^c using a fully connected layer. The resulting state embedding \mathbf{z}_t is obtained by the addition of these input embedding. Formally, we define the state encoder of the current state $\mathcal{X}_t = (\mathbf{X}_t, s_t, \mathbf{c}_t)$, parameterized by θ , as

$$e_\theta : \mathbb{R}^{|\mathbf{X}_t| \times W \times H \times 3} \times \mathbb{R} \times \mathbb{R}^k \rightarrow \mathbb{R}^{S \times c} . \quad (2)$$

In CIL [8] and CILRS [9], \mathbf{c}_t is treated as a switcher (condition) to trigger different MLP branches for predicting \mathbf{a}_t . Here we treat \mathbf{c}_t as an input signal to be later processed by a transformer. This is because we have not observed obvious differences between these two approaches while treating \mathbf{c}_t as input signal simplifies the training.

3.2.2 Attention Learning

To naturally associate intra-view and inter-view information, we adopt the self-attention mechanism from the transformer model [30]. Our intention of using the self-attention mechanism is that it can be effective to learn the mutual relevance between tokens that are spatially far away, and this will help our model to associate feature map patches (tokens) across different views (*i.e.*, coming from visual information to the left, center, and right from the ego-vehicle).

Over the embedded space \mathbf{Z}_t , we learn a scene embedding using a transformer encoder that consists of L multi-head self-attention layers. Each one includes Multi-headed Self-Attention (MHSA) [30], layer normalization (LN) [1], and feed-forward MLP blocks. The final output is a linear projection of the concatenated output of each attention head, which is then fed into the action prediction module, which is an MLP. We use $L = 4$ layers, with 4 heads each. The hidden dimension D of the transformer layer is set to be equal to the ResNet output dimension, *i.e.*, $D = 512$.

3.2.3 Action Prediction

For predicting the action, the output of the transformer encoder with a size of $S \times c$ is average pooled and fed into an MLP. The MLP consists of three fully connected layers (FC) with ReLu non-linearity applied between each FC. The

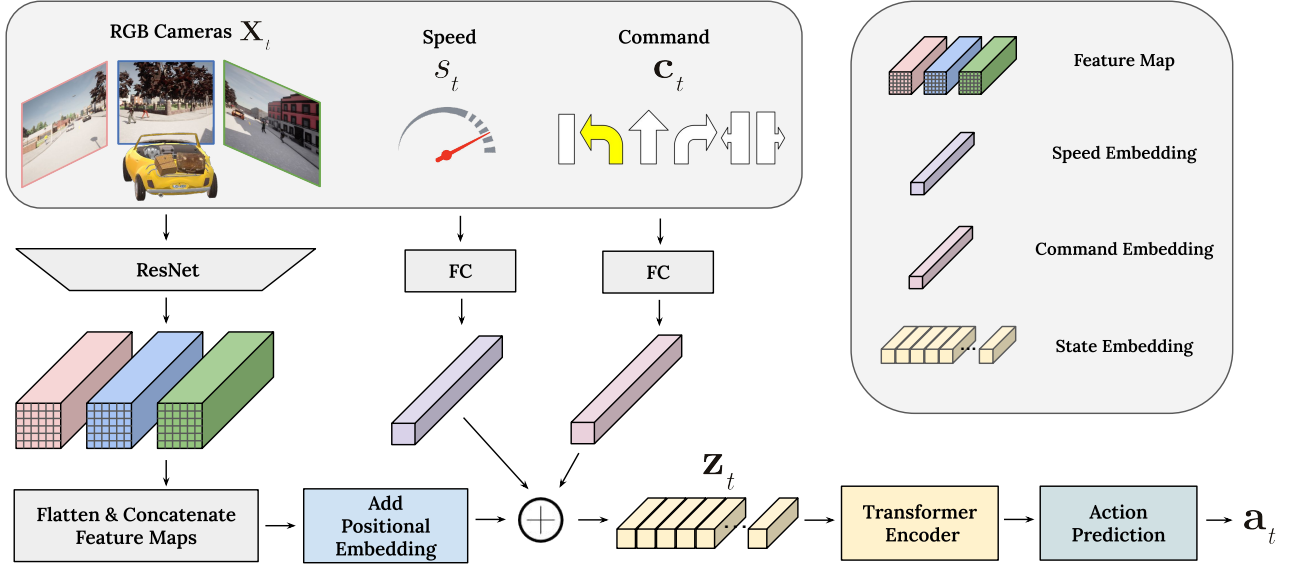


Figure 1. CIL++’s architecture: our model is mainly comprised of three parts: state embedding, transformer encoder and action prediction. Specifically, the input observation consists of multi-view RGB images X_t , ego-vehicle’s speed s_t , and high-level navigation command c_t . The output is action a_t , which is directly applied to maneuver the ego-vehicle. Since a_t consists of the ego-vehicle’s steering angle and acceleration, CIL++ is an EtE-AD model trained with self-supervision. Note that these action components are automatically read and associated to the captured images during data collection.

final output action $\mathbf{a}_t \in \mathbb{R}^2$ comprises of the steering angle and acceleration (brake/throttle), *i.e.*, $\mathbf{a}_t = (a_{s,t}, a_{acc,t})$.

3.3. Loss Function

At time t , given a predicted action \mathbf{a}_t and a ground truth action $\hat{\mathbf{a}}_t$, we define the training loss as:

$$\mathcal{L}(\mathbf{a}_t, \hat{\mathbf{a}}_t) = \lambda_{acc} \|a_{acc,t} - \hat{a}_{acc,t}\|_1 + \lambda_s \|a_{s,t} - \hat{a}_{s,t}\|_1, \quad (3)$$

where $\|\cdot\|_1$ is the L_1 distance, λ_{acc} and λ_s indicate the weights given to the acceleration and steering angle loss, respectively. In our case, we consider steering angle and acceleration to be both in the range of $[-1, 1]$. Negative values of the acceleration correspond to braking, while positive ones to throttle. The weights are set to $\lambda_{acc} = \lambda_s = 0.5$.

In CILRS [9], speed prediction regularization is applied in the training loss to avoid the inertia problem caused by the overwhelming probability of ego staying static in the training data. We do not observe this problem in our case, thus the speed prediction branch is not applied in our setting. Our result suggests that a simple L_1 loss is able to provide compelling performance, even in a new town.

4. Implementation

4.1. Datasets

In order to conduct our experiments, we use the latest version of CARLA simulator [13], *i.e.*, 0.9.13. As re-

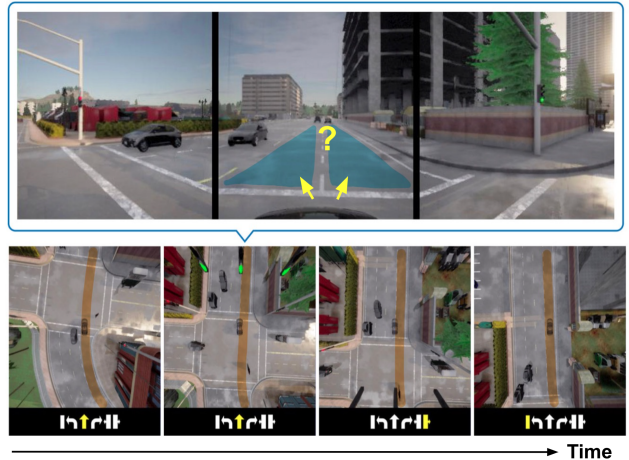


Figure 2. Top: when the ego-vehicle is entering to a new road segment from an intersection, the *go-straight* navigation command is ambiguous. The ego-vehicle can legally move to any of the highlighted lanes. Bottom: four aerial views at different times with the pre-planned global trajectory shown in orange. They illustrate how the high-level navigation command changes to *move-to-right-lane*, to inform how to get back to the desired trajectory.

cent top-performing methods [16], for on-board data collection in CARLA, we use the *teacher* expert driver from [34], termed as Roach RL since it is based on reinforce-

ment learning and was trained with privileged information. Roach RL shows a more realistic and diverse behavior than the default (handcrafted) expert driver in CARLA. Note that in real-world experiments we would use different human drivers as experts. We use the default settings of [34], so as in the *student* driver of [34] (RIM) as well as in [16] (MILE), the ego-vehicle is the Lincoln 2017 available in CARLA. Each of our three forward-facing cameras on-board the ego-vehicle has a resolution of $W \times H = 300 \times 300$ pixels, covering an HFOV of 60° . They are placed without overlapping so that they jointly cover an HFOV= 180° centered in the main axis of the ego-vehicle.

With such expert driver, ego-vehicle, and on-board cameras, we collect data for increasingly complex experiments. First, we collect a dataset from Town01 in CARLA, which is a small town only enabling single-lane driving, *i.e.*, lane change maneuvers are not possible. In particular, we collect 15 hours of data at 10 fps (~ 540 K frames from each camera view), under 4 training weathers, namely, ClearNoon, ClearSunset, HardRainNoon, and WetNoon. In this case, CARLA’s Town02 is used for generalization testing under SoftRainSunset and WetSunset weather conditions. Second, we collect a dataset from multiple CARLA’s towns so including more complex scenarios such as multi-lane driving, entering and exiting highways, passing crossroads, *etc.* In order to keep the same setting as [16], we hold Town05 for testing, and collect 25 hours of data at 10 fps from Town01 to Town06 (5 hours per town; ~ 900 K frames from each camera). Training and testing weathers are the same for both Town01 and Town02. More details about our datasets are provided in the supplementary.

4.2. High-level Navigation Commands

As in CILRS [9], at training time we use simple navigation commands such as *continue* in lane, or *go-straight/turn-left/turn-right* next time an intersection is reached. However, in complex towns, after crossing an intersection in any direction, we may legally enter any of multiple lanes. Thus, since this can be known by the global navigation system, when the ego-vehicle enters a lane out of the pre-planned global trajectory, a corrective command is forced, like *move-to-left-lane* or *move-to-right-lane* as soon as possible. This corrective mechanism is used only at testing time. Figure 2 provides an example.

4.3. Training Details

To optimize Eq. (3), we use the Adam [17] with an initial learning rate of 10^{-4} and weight decay of 0.01. We train for 80 epochs on 2 NVIDIA A40 GPUs in parallel, with a batch size of 120. The learning rate decays by half at epochs 30, 50, and 65. More training details can be found in the supplementary material.

5. Driving Evaluation Metrics

We follow the *NoCrash* benchmark [9] and the offline CARLA leaderboard benchmark [16, 34] for experiments on small single-lane towns (Sec. 6.1) and multiple towns (Sec. 6.2), respectively.

NoCrash Metrics. It consists of three tasks with increasing levels of difficulty: *empty*, *regular*, and *dense*, according to the number of dynamic objects (traffic density) in the scene (*i.e.*, pedestrians and vehicles). In the *dense* case, the default traffic density set in NoCrash always leads to congestion deadlocks at intersections [34]. Thus, we follow the *busy* case as redefined in [34]. Each task corresponds to 25 goal-directed episodes under 2 new kinds of weather. The episode will be terminated and counted as failure once a collision occurs. For the other infractions, the driving score will be deduced according to the penalty rule in NoCrash.

The main metric to compare driving models is the success rate (*SR*), which is the percentage of episodes successfully completed. For a fine-grained comparison, in addition, we provide the strict success rate (*S.SR*). It reflects the percentage of successful episodes under zero tolerance for any traffic infraction, such as not stopping at red traffic lights, route deviation, *etc.*. As a complement, we also include additional infraction metrics: *TL* is the number of times not stopping at a red traffic light; *CV* is the number of collisions with other vehicles; *R.Dev* is the number of route deviations, *i.e.*, when the high-level command is not well-executed; *OL* accounts for the ego-vehicle driving out-of-lane (*e.g.*, in the opposite lane or in the sidewalk); *CL* is the number of collisions with the layout. All infraction values are normalized per kilometer.

Offline Leaderboard Metrics. To align our evaluation with [16], we use the offline CARLA’s Leaderboard metrics for multiple towns. The most important are the average driving score (*Avg.DS*) and the average route completion (*Avg.RC*). *Avg.DS* is based on penalizing driving performance according to the terms defined in CARLA’s Leaderboard, while *Avg.RC* is the average distance towards the goal that the ego-vehicle is able to travel.

6. Results

We compare CIL++ with two SOTA vision-based EtE-AD models, namely, the Roach IL model (here RIM) [34] and MILE [16]. CIL++ does not require supervision for training. In contrast, MILE is trained with semantic BeV as supervision, while RIM requires teaching from the Roach RL expert trained with privileged information.

	Empty			Regular			Busy		
	↑ SR(%)	↑ S.SR(%)	↓ T.L	↑ SR(%)	↑ S.SR(%)	↓ T.L	↑ SR(%)	↑ S.SR(%)	↓ C.V
RIM	100 ± 0.0	85 ± 1.2	66 ± 5.0	97 ± 2.3	86 ± 7.2	66 ± 5.4	81 ± 5.0	68 ± 7.2	63 ± 52.7
CIL++	100 ± 0.0	100 ± 0.0	0 ± 0.0	99 ± 2.3	97 ± 3.1	7 ± 7.9	83 ± 7.6	77 ± 7.6	45 ± 21.5
Expert	100 ± 0.0	100 ± 0.0	0 ± 0.0	100 ± 0.0	97 ± 0.0	13 ± 4.6	84 ± 2.0	82 ± 2.0	37 ± 14.1

Table 1. Town02 NoCrash results. RIM stands for Roach IL and the Expert is Roach RL [34]. All models are tested on CARLA 0.9.13. Mean and standard deviations are computed using three runs with different seeds. For ↑, the higher the better, while for ↓ is the opposite.

	↑ SR(%)	↑ S.SR(%)	↑ Avg.RC(%)	↑ Avg.DS	↓ C.L	↓ T.L	↓ O.L	↓ R.Dev
HFOV 100°	52	40	83	69.1	428.6	19.6	339.6	10.7
HFOV 180°	100	98	100	99.2	7.3	0.0	0.0	0.0
Expert	100	100	100	100.0	0.0	0.0	0.0	0.0

Table 2. Impact of sensor suite HFOV in the NoCrash regular case. For HFOV=100° we use a single camera with a resolution of $W \times H = 600 \times 170$ pixels, while for HFOV=180° we use the multi-view setting detailed in the main text.



(a) Roach RL [34]: using semantic BeV as input during training time



(b) CIL++: only images from three views as input

Figure 3. Top Left: The expert we use for data collection is (the teacher) Roach RL [34], which has access to semantic BeVs. Top Right: Using an insufficient FOV, the red traffic light is not observable in the image when the expert stops close to it, which may cause causal confusion when applying imitation learning to train (the student) RIM. Bottom: CIL++ avoids this causal confusion by using a larger HFOV based on three complementary images (from different cameras). More specifically, RIM uses HFOV=100°, while CIL++ uses HFOV=180°.

6.1. Small Single-lane Towns

We first use CARLA’s Town01 and Town02 along with the NoCrash metrics (Sec. 5) for initial experiments. Town01 is used for training and Town02 for testing (Sec. 4.1). There is no MILE model checkpoint trained only on Town01. MILE is trained on CARLA’s multiple towns, while RIM has versions trained on Town01 and multiple towns. Thus, for a fair comparison, in this evaluation, we only use RIM’s single town trained model. We show in

Table 1 SR and S.SR for the considered traffic densities (empty, regular, busy). In order to have a more focused evaluation, we show T.L only for the empty and regular cases, while C.V is shown only for the busy case. Note that scenarios with no or few dynamic obstacles can better show the ego-vehicle reaction to red traffic lights, while collisions are better evaluated in scenarios with more dynamic objects.

In general, CIL++ achieves the best results in all the tasks. In the empty case, CIL++ clearly outperforms RIM in avoiding traffic light infractions, which also contributes to a better S.SR. In the regular case, we reach the same conclusion. In the busy case, where even the expert is underperforming, CIL++ reaches almost its performance, again, being clearly better than RIM for S.SR and producing fewer collisions with vehicles. For the expert, the failure cases in busy scenarios are due to traffic deadlocks, which lead to a timeout in route completion. Thus, its performance still can be considered as a proper upper bound.

Traffic lights tend to be on sidewalks, so detecting them from a close distance requires a sensor setting with a proper HFOV. Otherwise, causal confusion can appear. We think that the poor performance of RIM on the T.L metric is due to a narrow HFOV as illustrated in Fig. 3. To confirm this hypothesis, we conduct experiments using two HFOV settings for CIL++, 100 and 180. The results are reported in Table 2. Note how by using HFOV=100°, more infractions (T.L, C.L, O.L, R.Dev) are observed than by using HFOV=180°. For HFOV=100°, we have observed that the track of the road shoulder is easily out-of-observation at intersections, leading to more O.L, C.L, and R.Dev. For HFOV=180°, the ego-vehicle can better perform the right driving maneuver, thanks to having the road shoulder as a reference.

	↑ Avg.RC(%)	↑ Avg.DS	↓ C.V	↓ C.L	↓ T.L	↓ O.L	↓ R.Dev
RIM	92 ± 3.1	51 ± 7.9	7.5 ± 1.3	4.3 ± 1.6	26.0 ± 8.9	5.4 ± 2.7	3.0 ± 3.2
MILE	98 ± 2.2	73 ± 2.9	6.0 ± 3.7	0.0 ± 0.0	3.6 ± 3.8	3.5 ± 1.5	0.0 ± 0.0
CIL++	98 ± 1.7	68 ± 2.7	6.0 ± 0.5	3.8 ± 0.7	5.8 ± 5.1	6.1 ± 2.2	9.4 ± 3.6
Expert	99 ± 0.8	89 ± 1.7	3.2 ± 1.1	0.0 ± 0.0	1.3 ± 0.4	0.0 ± 0.0	0.0 ± 0.0

Table 3. Town05 results according to CARLA’s offline metrics. All models are tested on CARLA 0.9.13. Mean and standard deviations are computed using three runs with different seeds. For ↑, the higher the better, while for ↓ is the opposite.

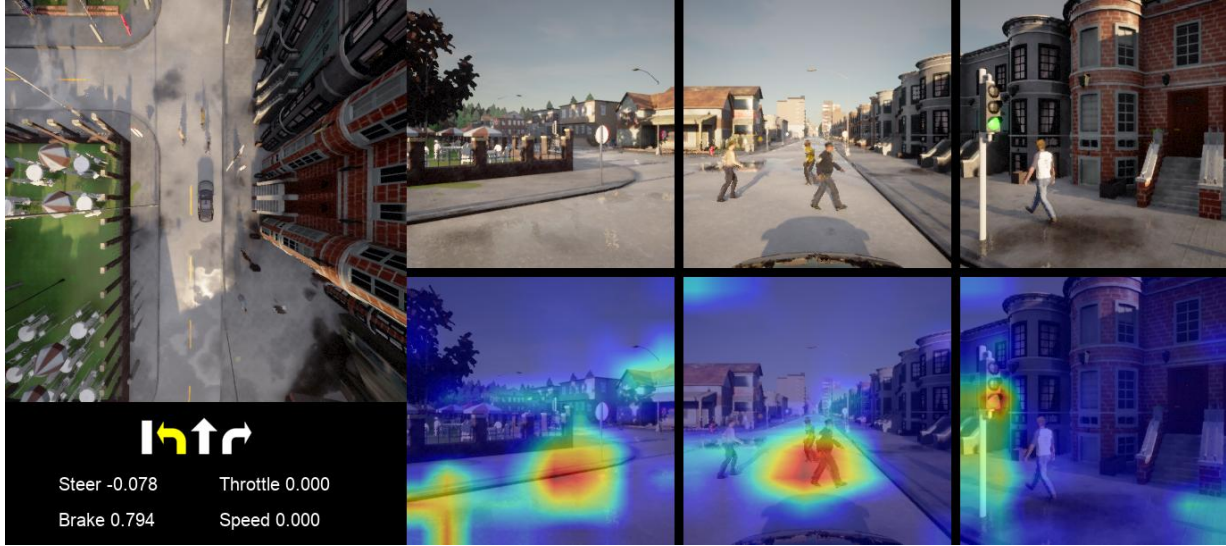


Figure 4. Activation maps of CIL++ at an intersection in Town02. Three image areas from different views are highly activated: the traffic light at the right image, the crossing pedestrians at the central one, and the lane shoulder at the left one. Causality between observation and action is shown as a strong braking (0.794) due to the pedestrians, even though the traffic light in green and the *turn-left* command.

	↑ SR(%)	↑ S.SR(%)	↑ Avg.RC(%)	↑ Avg.DS
LF.A	72	62	86	78.1
LF.C	76	66	88	80.6
Token	88	80	93	88.4
CIL++	88	84	93	88.8

Table 4. Results of different data input fusion approaches for busy scenarios.

	↑ SR(%)	↑ S.SR(%)	↑ Avg.RC(%)	↑ Avg.DS
GAP	64	46	87	75.1
VS	70	62	89	78.6
CIL++	88	84	93	88.8

Table 5. Results of different multi-view fusion approaches for busy scenarios.

	↑ SR(%)	↑ S.SR(%)	↑ Avg.RC (%)	↑ Avg.DS
M.C	100	96	100	98.9
A.E	98	98	99	98.3
B.G	86	84	96	91.7
L.C	100	100	100	100.0

Table 6. Deploying CIL++ in new vehicle models. L.C: Lincoln (vehicle used for training CIL++); M.C: Mini Cooper; A.E: Audi Etron; B.G: BMW Grand Tourer.

6.2. Multi-town Generalization

In this section, we assess the performance of CIL++ in much more complex scenarios, as provided by CARLA’s multiple towns. As mentioned in Sec. 4.1, for a fair comparison, we align the training and testing settings with MILE [16], using CARLA’s offline Leaderboard metrics (Sec. 5). The results for all models trained on multi-town data are shown in 3 RIM shows the worst performance among the three models, incurring more infractions,

thus obtaining a significantly lower Avg.DS score. CIL++ achieves 98% Avg.RC, which is on par with MILE. In terms of Avg.DS, MILE remains the best scoring, yielding a 73% while CIL++ achieves a 68%. We observe that this is because MILE seldom drives outside the pre-planned lane, given the route map as input. On the contrary, CIL++ lacks the explicit use of this route map since it only receives high-level navigation commands.

6.3. Visualizing CIL++’s Attention

We are interested in the image content to which CIL++ pays attention. Following Grad-CAM [24], gradients flow from the action space to the final convolutional layer of the ResNet backbone. This should produce a map that highlights the important image areas for action prediction. However, since CIL++ solves a regression task, its output could be either negative or positive values, while Grad-CAM is originally designed for image classification tasks which always provide positive outputs. To adapt Grad-CAM to our case, we cannot merely take into account the positive gradient of the feature map. The computation should be divided into two cases depending on the sign of the output value. Negative gradients are used to calculate the weights for the feature map when the acceleration or steering angle value is lower than zero, otherwise, the positive gradient is used.

Fig. 4 shows the activation map at an intersection. Three image areas are highly activated: the traffic light at the right image, the crossing pedestrians at the central one, and the lane shoulder at the left one. Thus, we believe that CIL++ shows a proper understanding of this scene, and a clear causality between observation and action since it decides to brake due to the pedestrians, even though the traffic light is in green and a *turn-left* navigation command is given.

7. Ablation Study

To inspect the impact of some components of CIL++, we provide an ablation study. We are interested in the fusion of input data, in multi-view fusion, and deployment in different vehicle models without retraining.

7.1. Input Data Fusion

EtE-AD models require not only sensor data but also signal information, like the ego-vehicle speed and a high-level navigation command. It is interesting to study how to properly fuse these inputs. To compare, we implement several types of input data fusion in Table 4: adding, concatenation, and tokenization. In the first, the speed and command features are simply added to the image features. This addition could be done either before the transformer block (the default operation in CIL++), or after. We name the latter as late fusion adding (LFA) in the table. Another common data fusion method is concatenation, which firstly stacks all the features and takes an extra join FC layer

to fuse them, which we term as late fusion concatenation (LFC) in the table. Since the transformer model uses a self-attention mechanism to fuse features between tokens, we can tokenize the speed and navigation command features and feed them into the transformer block along with the image features. We term this approach as Token in the table. Our results suggest that there is no obvious difference between tokenization and early adding fusion. These two approaches show better results than the late fusion.

7.2. Multi-view Fusion

CIL++ uses self-attention layers to fuse multi-view information. To understand the effect of the self-attention mechanism, we remove the transformer block and simply use the ResNet34 which retains the average pooling and an FC layer for embedding each image view. The embedding outputs are then stacked and fed to the FC join layers for fusion. We term this approach as view stacking (VS) in Table 5. The speed and command features are added to the joint embedding before feeding into the action prediction MLP. We could see that without the self-attention layers, the SR drops from 88% to 70%. We think this is because the average pooling layer causes a loss of spatial information, while this information is very important for actual driving. The agent should take different actions according to the location of dynamic obstacles. We also use a transformer block to process the output of the ResNet average pooling layer (GAP), instead of using the flattened feature map from the last convolutional layer of ResNet34. The results drop significantly, *e.g.*, the SR goes from 88% to 64%.

7.3. Deploying on New Vehicles

Compared to CIL++, some works (*e.g.*, [5–7,23]) predict waypoints, which are later transformed into a parametric trajectory to be followed by the action of an additional low-level controller. This approach may require a significant parameter tuning, specially for adaptation to new vehicle models. Since CARLA 0.9.13 simulates different vehicle dynamics, we can now explore the inter-vehicle transferability of CIL++. Thus, we replicate the multi-view camera suite in a new vehicle, but we do not retrain CIL++. Accordingly, we use new vehicle models with different dynamics. Table 6 shows the obtained results for regular scenarios in Town02. We can see that there is not a significant performance drop, drawing the possibility of deploying CIL++ on new types of vehicles without the need for additional training. This is so provided the new vehicle is of a similar category to the one in which CIL++ was trained (*e.g.*, from a van model to another, but not to a heavy truck).

8. Conclusions

We have presented CIL++, which aims at becoming a new strong baseline representing EtE-AD models trained

by self-supervised imitation learning. This is required because recent literature may lead to the conclusion that such approaches are poorly performing compared to those relying on additional and costly supervision. We have argued that previous self-supervised EtE-AD models were developed in sub-optimal conditions. Thus, we have developed a model which relies on three cameras (views) to reach an HFOV=180° and a more realistic expert driver to collect on-board data in CARLA simulator. We have proposed a visual transformer that acts as a mid-level attention mechanism for these views, so allowing CIL++ to associate feature map patches (tokens) across different views. CIL++ performs at expert level on NoCrash metrics and is a self-supervised EtE-AD model capable of obtaining competitive results in complex towns. The supplementary material presents results on more metrics. We have presented an ablation study showing the relevance of all the components of CIL++, even showing transferability among similar types of vehicles without retraining. In future work, we plan to add rear-view cameras, to improve on lane changes.

References

- [1] Jimmy Lei Ba, Jamie Ryan Kiros, and Geoffrey E Hinton. Layer normalization, 2016. [3](#)
- [2] Mayank Bansal, Alex Krizhevsky, and Abhijit S. Ogale. ChauffeurNet: Learning to drive by imitating the best and synthesizing the worst. In *Robotics: Science and Systems (RSS)*, 2019. [2](#)
- [3] Mariusz Bojarski, Davide Del Testa, Daniel Dworakowski, Bernhard Firner, Beat Flepp, Praseoon Goyal, Lawrence D. Jackel, Mathew Monfort, Urs Muller, Jiakai Zhang, Xin Zhang, Jake Zhao, and Karol Zieba. End to end learning for self-driving cars. arXiv:1712.00409, 2016. [2](#)
- [4] M. Bojarski, P. Yeres, A. Choromanska, K. Choromanski, B. Firner, L. Jackel, and U. Muller. Explaining how a deep neural network trained with end-to-end learning steers a car. arXiv:1704.07911, 2017. [2](#)
- [5] Dian Chen and Philipp Krähenbühl. Learning from all vehicles. In *Int. Conf. on Computer Vision and Pattern Recognition (CVPR)*, 2022. [1, 2, 8](#)
- [6] Dian Chen, Brady Zhou, Vladlen Koltun, and Philipp Krähenbühl. Learning by cheating. In *Conf. on Robot Learning (CoRL)*, 2019. [1, 2, 8](#)
- [7] Kashyap Chitta, Aditya Prakash, and Andreas Geiger. NEAT: Neural attention fields for end-to-end autonomous driving. In *Inter. Conf. on Computer Vision (ICCV)*, 2021. [1, 2, 3, 8](#)
- [8] Felipe Codevilla, Matthias Müller, Antonio M. López, Vladlen Koltun, and Alexey Dosovitskiy. End-to-end driving via conditional imitation learning. In *Inter. Conf. on Robotics and Automation (ICRA)*, 2018. [2, 3](#)
- [9] Felipe Codevilla, Edgar Santana, Antonio M. López, and Adrien Gaidon. Exploring the limitations of behavior cloning for autonomous driving. In *Inter. Conf. on Computer Vision (ICCV)*, 2019. [1, 2, 3, 4, 5](#)
- [10] Pim De Haan, Dinesh Jayaraman, and Sergey Levine. Causal confusion in imitation learning. In *Neural Information Processing Systems (NeurIPS)*, 2019. [1](#)
- [11] Jia Deng, Wei Dong, Richard Socher, Li-Jia Li, Kai Li, and Li Fei-Fei. ImageNet: A large-scale hierarchical image database. In *Int. Conf. on Computer Vision and Pattern Recognition (CVPR)*, 2009. [3](#)
- [12] Alexey Dosovitskiy, Lucas Beyer, Alexander Kolesnikov, Dirk Weissenborn, Xiaohua Zhai, Thomas Unterthiner, Mostafa Dehghani, Matthias Minderer, Georg Heigold, Sylvain Gelly, Jakob Uszkoreit, and Neil Houlsby. An image is worth 16x16 words: Transformers for image recognition at scale. In *Inter. Conf. on Learning Representation (ICLR)*, 2021. [3](#)
- [13] Alexey Dosovitskiy, German Ros, Felipe Codevilla, Antonio López, and Vladlen Koltun. CARLA: An open urban driving simulator. In *Conf. on Robot Learning (CoRL)*, 2017. [2, 4](#)
- [14] Sorin Grigorescu, Bogdan Trasnea, Tiberiu Cocias, and Gigel Macesanu. A survey of deep learning techniques for autonomous driving. *Journal of Field Robotics*, 37(3):362–386, 2020. [1](#)
- [15] Kaiming He, Xiangyu Zhang, Shaoqing Ren, and Jian Sun. Deep residual learning for image recognition. In *Int. Conf. on Computer Vision and Pattern Recognition (CVPR)*, 2016. [3](#)
- [16] Anthony Hu, Gianluca Corrado, Nicolas Griffiths, Zak Murez, Corina Gurau, Hudson Yeo, Alex Kendall, Roberto Cipolla, and Jamie Shotton. Model-based imitation learning for urban driving. In *Neural Information Processing Systems (NeurIPS)*, 2022. [1, 2, 4, 5, 7](#)
- [17] Diederik P Kingma and Jimmy Ba. Adam: A method for stochastic optimization. In *Inter. Conf. on Learning Representation (ICLR)*, 2015. [5](#)
- [18] Yann LeCun, Urs Muller, Jan Ben, Eric Cosatto, and Beat Flepp. Off-road obstacle avoidance through end-to-end learning. In *Neural Information Processing Systems (NIPS)*, 2005. [2](#)
- [19] Xiaodan Liang, Tairui Wang, Luona Yang, and Eric Xing. CIRL: Controllable imitative reinforcement learning for vision-based self-driving. In *European Conf. on Computer Vision (ECCV)*, 2018. [1, 2](#)
- [20] Matthias Mueller, Alexey Dosovitskiy, Bernard Ghanem, and Vladlen Koltun. Driving policy transfer via modularity and abstraction. In *Conf. on Robot Learning (CoRL)*, 2018. [1, 2](#)
- [21] Yunpeng Pan, Ching-An Cheng, Kamil Saigol, Keuntaek Lee, Xinyan Yan, Evangelos A Theodorou, and Byron Boots. Agile autonomous driving using end-to-end deep imitation learning. In *Robotics: Science and Systems (RSS)*, 2018. [2](#)
- [22] Dean Pomerleau. ALVINN: An autonomous land vehicle in a neural network. In *Neural Information Processing Systems (NIPS)*, 1989. [2](#)
- [23] Aditya Prakash, Kashyap Chitta, and Andreas Geiger. Multi-modal fusion transformer for end-to-end autonomous driving. In *Int. Conf. on Computer Vision and Pattern Recognition (CVPR)*, 2021. [1, 2, 8](#)
- [24] Ramprasaath R Selvaraju, Michael Cogswell, Abhishek Das, Ramakrishna Vedantam, Devi Parikh, and Dhruv Batra. Grad-cam: Visual explanations from deep networks via gradient-based localization. In *Inter. Conf. on Computer Vision (ICCV)*, 2017. [8](#)
- [25] Hao Shao, Letian Wang, Ruobing Chen, Hongsheng Li, and Yu Liu. InterFuser: Safety-enhanced autonomous driving using interpretable sensor fusion transformer. In *Conf. on Robot Learning (CoRL)*, 2022. [1, 2](#)
- [26] Jonathan Spencer, Sanjiban Choudhury, Arun Venkatraman, Brian Ziebart, and J Andrew Bagnell. Feedback in imitation learning: The three regimes of covariate shift. arXiv:2102.02872, 2021. [1](#)
- [27] Ardi Tampuu, Tabet Matiisen, Maksym Semikin, Dmytro Fishman, and Naveed Muhammad. A survey of end-to-end driving: Architectures and training methods. *IEEE Trans. on Neural Networks and Learning Systems*, 33(4):1364–1384, 2022. [1, 2](#)
- [28] Learning to drive from simulation without real world labels. Bewley, alex and rigley, jessica and liu, yuxuan and hawke, jeffrey and shen, richard and lam, vinh-dieu and kendall, alex. In *Inter. Conf. on Robotics and Automation (ICRA)*, 2019. [2](#)
- [29] Marin Toromanoff, Emilie Wirbel, and Fabien Moutarde. End-to-end model-free reinforcement learning for urban

- driving using implicit affordances. In *Int. Conf. on Computer Vision and Pattern Recognition (CVPR)*, 2020. [1](#)
- [30] Ashish Vaswani, Noam Shazeer, Niki Parmar, Jakob Uszkoreit, Llion Jones, Aidan N Gomez, Łukasz Kaiser, and Illia Polosukhin. Attention is all you need. In *Neural Information Processing Systems (NeurIPS)*, 2017. [2](#), [3](#)
- [31] Penghao Wu, Xiaosong Jia, Li Chen, Junchi Yan, Hongyang Li, and Yu Qiao. Trajectory-guided control prediction for end-to-end autonomous driving: A simple yet strong baseline. In *Neural Information Processing Systems (NeurIPS)*, 2022. [1](#), [2](#)
- [32] Yi Xiao, Felipe Codevilla, Akhil Gurram, Onay Urfalioglu, and Antonio M López. Multimodal end-to-end autonomous driving. *IEEE Trans. on Intelligent Transportation Systems*, 23(1):537–547, 2020. [2](#)
- [33] Ekim Yurtsever, Jacob Lambert, Alexander Carballo, and Kazuya Takeda. A survey of autonomous driving: Common practices and emerging technologies. *IEEE Access*, 8:58443–58469, 2020. [1](#)
- [34] Zhejun Zhang, Alexander Liniger, Dengxin Dai, Fisher Yu, and Luc Van Gool. End-to-end urban driving by imitating a reinforcement learning coach. In *Inter. Conf. on Computer Vision (ICCV)*, 2021. [1](#), [2](#), [4](#), [5](#), [6](#)

Supplementary Material for “Scaling Self-Supervised End-to-End Driving with Multi-View Attention Learning”

In our supplementary, we provide the extra detailed information about our work, which could be mainly concluded in three sections: the data collection in Section 1, the details of our training setup in Section 2, and the additional evaluation results in Section 3. In Section 4, we introduce the CARLA simulator platform and scenario runner that we used for our experiments. We also provide a video named *driving.mp4* to demonstrate the driving performance of CIL++.

1. Dataset Collection

To collect our training dataset, we deploy the Reinforcement Learning agent from Roach [34] in the CARLA simulator [13], attaching a sensor suite that will record the environment at specific timesteps. In this section, we briefly summarize the used settings for the expert agent, and provide complete parameter settings in the table.

Sensor Configuration We use three front cameras (giving us three views: left, central, and right), all located at the same position and with the same horizontal field of view (HFOV) of 60° . The cameras were positioned to cover the full 180° HFOV in front of the ego vehicle, without overlapping. Full details on the sensor configuration can be found in Table 1.

Data Episodes For each episode, we spawn the expert vehicle and its attached sensor suite in a random location on each map and assign a random route to it. The expert will follow this route until it has driven for the predefined episode duration. Each town has a random range where the number of pedestrians and vehicles will be (uniformly) drawn from. The route settings and towns used to collect the dataset are further detailed in Table 1.

Data Distribution In Figure 1, we show the data distributions for both the steering angle and acceleration, for the datasets collected for training CIL++. The two datasets are of 15 and 25 hours of driving, corresponding, respectively, to the smaller, single-lane towns and multi-lane towns.

The road layouts of each town mainly influence the steering angle distribution. The concentration around 0.0 of

steering angle for both datasets is due to the fact that most of the driving is done following the straight lane, *i.e.* in the towns used, the roads are mainly comprised of straight roads. Note that all of the towns in CARLA are designed with right-hand traffic, that is, in bidirectional traffic, the ego vehicle drives on the right side of the road. This results in right turns needing a higher steering angle (turning radius will be small) and left turns needing a lower steering angle (turning radius will be large).

In contrast, the acceleration distribution is mainly affected by other dynamic objects in the scene. Concretely, the red traffic light or Stop sign, pedestrians crossing the road, and other leading vehicles will force the expert vehicle to stop or adjust its speed, hence leading to the large concentration around -1.0 in the acceleration distribution for both datasets. The other concentrations around 1.0 and 0.4 are the acceleration after coming to a stop (either by blockage by other dynamic objects or traffic lights/Stop signs) and the acceleration needed to maintain a constant driving speed.

2. Training Details

Details on the training hyperparameters can be found in Table 2. For a more in-depth look into the architecture, Table 3 presents the input and output dimensions of each module used in our entire pipeline. The pipeline flow is row-wise, that is, we start with 3 RGB images at 300×300 resolution, and our final output is of shape 1×2 , corresponding to the throttle and steering angle that the ego vehicle should apply at the given timestep.

3. Additional Evaluation Results

In this section, we provide the full-benchmark results on the extra statistic metrics from CARLA simulator.

3.1. Experimental Setting

We compare CIL++ with two SOTA vision-based EtE-AD models, namely, the Roach IL model (RIM) [34] and MILE [16]. We measure the performance of the models on two experiments with different scale: single-lane small-town and multi-lane town. As we mentioned in our main paper, MILE is trained on multiple towns in CARLA, whereas

	Item	Value			
RGB Cameras	views	3			
	Resolution	300 × 300			
	Field of view	60°			
	Camera position (x, y, z)	(0.0, 0.0, 2.0)			
	Camera rotation (ϕ, θ, ψ)	View	Roll	Pitch	Yaw
		left	0.0°	0.0°	−60.0°
		central	0.0°	0.0°	0.0°
		right	0.0°	0.0°	60.0°
	Lens circle	None			
	Frequency	10 Hz			
Episode	Dynamic Objects (random choice)	Town	Pedestrians	Vehicles	
		Town01	$\mathcal{U}(80, 160)$	$\mathcal{U}(80, 160)$	
		Town02	$\mathcal{U}(60, 80)$	$\mathcal{U}(60, 80)$	
		Town03	$\mathcal{U}(50, 120)$	$\mathcal{U}(50, 120)$	
		Town04	$\mathcal{U}(40, 160)$	$\mathcal{U}(60, 160)$	
		Town06	$\mathcal{U}(60, 160)$	$\mathcal{U}(60, 160)$	
	Episode duration	300 s			
	Spawn point	Random			
	Route plan	Random			
	Pedestrian crossing factor	1.0			

Table 1. Camera and episode settings used for data collection with the expert driver.

RIM has different versions, each trained on different set of towns (only Town01 and another on multiple towns). Thus, in single-lane small-town experiment, we only use RIM’s single town trained model for comparison. In multi-lane town experiment, we compare CIL++ with both RIM and MILE. All models are tested on CARLA 0.9.13. The Expert is Roach RL agent [34], and we repeat each experiment 3 times with a different random seed.

Single-lane Small-town Experimental Setting We follow the *NoCrash* benchmark setting, providing 4 sets of results:

- **Train Town & Train Weather:** 25 routes in Town01, on 4 training weather conditions: ClearNoon, ClearSunset, HardRainNoon, WetNoon
- **Train Town & New Weather:** 25 routes in Town01, on 2 new weather conditions: SoftRainSunset, WetSunset
- **New Town & Train Weather:** 25 routes in Town02, on 4 new weather conditions: ClearNoon, ClearSunset, HardRainNoon, WetNoon
- **New Town & New Weather:** 25 routes in Town02, on 2 new weather conditions: SoftRainSunset, WetSunset

Each of these sets consist of 3 tasks with increasing levels of difficulty: *Empty*, *Regular*, and *Dense*. We briefly explain them in the following:

- **Empty:** For both Town01 and Town02, the numbers of pedestrian and vehicle are set to 0/0.
- **Regular:** For Town01, the numbers of pedestrian/vehicle are set to 20/50. For Town02, the numbers of pedestrian and vehicle are set to 15/50.
- **Dense / Busy:** For Town01, the numbers of pedestrian/vehicle are set to 100/250. For Town02, the numbers of pedestrian and vehicle are set to 70/70.

Note that depending on the size of each town, the dynamic density (*i.e.* the numbers of pedestrian and vehicles) is varied. In addition, as we mentioned in our main paper, the original setting of the *NoCrash* benchmark on the dynamic density in Town02 is overloaded with dynamic agents, leading to many traffic deadlocks at the intersection. Hence we use *Busy* to replace *Dense*, in turn reducing the number of pedestrian from 140 to 70.

Multi-lane Town Experimental Setting We provide results in 2 settings:

- **Train Town & Train Weather:** 20 routes in Town03, on 4 training weather conditions: ClearNoon, ClearSunset, HardRainNoon, WetNoon
- **New Town & New Weather:** 10 routes in Town05, on 2 new weather conditions: SoftRainSunset, WetSunset

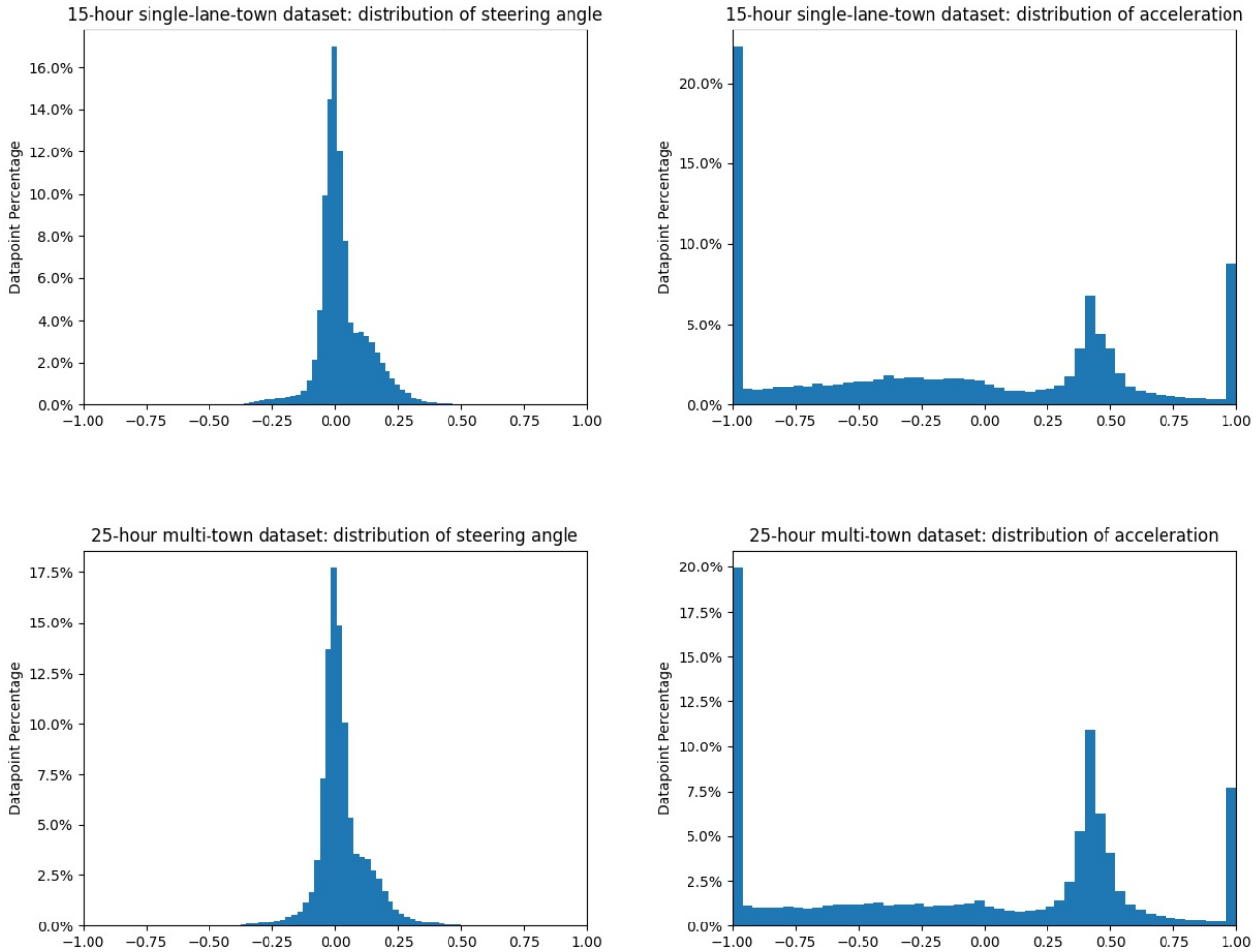


Figure 1. Data distribution for the two datasets collected for training CIL++. Regarding the steering angle and acceleration, negative values correspond to turning left and braking, and positive values correspond to turning right and accelerating, respectively.

The dynamic density is set to the same as the offline Leaderboard setting, which is a moderate level of traffic: For Town03, the numbers of pedestrian and vehicle are set to 70/70, while for Town05 they are set to 120/120.

Full Statistical Metrics In this section, we provide the explanation of the full statistical metrics on the CARLA simulator:

- **Success Rate (SR):** the percentage of episodes successfully completed.
- **Strict Success Rate (S.SR):** the percentage of episodes successfully completed, with zero tolerance for any traffic infraction
- **Average Route Completion (Avg.RC):** the average percentage of route completed by the driving agent
- **Average Driving Score (Avg.DS):** product of the route completion with infraction penalty defined on CARLA, averaged among all episodes
- **Collision on Pedestrian (C.P):** the number of collisions with pedestrians, normalized per kilometer. (penalty value: 0.50)
- **Collision on Vehicle (C.V):** the number of collisions with other vehicles, normalized per kilometer (penalty value: 0.60)
- **Collision on Layout (C.L):** the number of collisions with layout, normalized per kilometer (penalty value: 0.65)

Category	Name	Value
Training	GPUs	2×NVIDIA A40
	batch size	120
	seed	1314
	epochs	80
Optimizer	name	Adam
	weight decay	0.01
	β_1	0.9
	β_2	0.999
	ε	1×10^{-8}
	initial learning rate	1×10^{-4}
	learning rate decay	×0.5 at epochs 30, 50, and 65
Input image	resolution	300×300
	normalization	mean: [0.485, 0.456, 0.406] stdev: [0.229, 0.224, 0.225]
	pre-training	ImageNet
	Speed Input	normalization
Transformer	number of encoder layers	4
	heads per layer	4
Loss	action weights	$\lambda_{\text{acc}} = 0.5$ (acceleration) $\lambda_s = 0.5$ (steering angle)
	output ranges	steer angle [-1.0, 1.0] acceleration [-1.0, 1.0]

Table 2. Training hyperparameters of CIL++.

Module	Input size	Output size	Normalization	Non-linearity
ResNet34	$3 \times 300 \times 300 \times 3$	$3 \times 10 \times 10 \times 512$	BN	ReLU
Flatten	$3 \times 10 \times 10 \times 512$	300×512	/	/
Command	$1 \times 4 / 1 \times 6$	1×512	/	/
Speed	1	1×512	/	/
Element-wise addition	300×512		/	/
	1×512	300×512	/	/
	1×512		/	/
Positional Embedding	300×512	300×512	/	/
Transformer Encoder	300×512	300×512	LN	ReLU
Average Pooling	300×512	1×512	/	/
Action	1×512	1×512	/	ReLU
	1×512	1×256	/	ReLU
	1×256	1×2	/	/

Table 3. Architecture details of CIL++. Dimensions are per timestep and channel-last (*NHWC* or *NC*, when applicable). Dropout was not used in any layer or module (*i.e.*, set to 0.0 when applicable). For normalization, we use either BatchNorm (BN) or LayerNorm (LN) [1].

- **Traffic Light infraction (T.L)**: the number of times that the ego-vehicle does not stop at a red traffic light, normalized per kilometer (penalty value: 0.70)
- **Outside of Lane infraction (O.L)**: the percentage of the episode route that the ego-vehicle driving out-of-lane, normalized per kilometer
- **Route Deviation infraction (R.Dev)**: the number of the ego-vehicle does not follow the pre-planned high-level command. (penalty value: 0.90)
- **Timeout (T.O)**: a metric indicates that the ego-vehicle fails to complete the episode within the preset time.
- **Agent Block (A.B)**: a metric indicates that the ego-vehicle is blocked in the middle of the route.

Full NoCrash Experimental Results We provide the full *NoCrash* benchmark results among RIM, our CIL++ and expert: Train Town & Train Weather results in Table. 4, Train Town & New Weather results in Table. 5, New Town & Train Weather results in Table. 6 and New Town & New Weather results in Table. 7.

Full Multi-lane town Experimental Results We provide the multi-towns experimental results on two settings: Train Town & Train Weather in Table. 8 and New Town & New Weather results in Table. 9.

4. CARLA simulator: 0.9.13 (latest version)

For performing the driving evaluation, we updated the *NoCrash* benchmark to work with the latest CARLA version, 0.9.13. Given we have compared CIL++ with RIM and MILE, both of which were validated in CARLA 0.9.11, we provide some of the main differences between these two versions:

- Added new API function “set pedestrians seed” for better reproducibility. In our experiments, we keep the same pedestrian and traffic manager seeds for all models’ running.
- The default weather setting parameters (such as ClearNoon, ClearSunset, etc.) have been slightly changed between versions. We provide an example in Figure 2, showing some appearance differences of the same scene between these two versions under the same weather condition, ClearNoon. In Table 10 we show the changes in the weather parameters for each version of CARLA. In general, from the comparison of results in Table. 4 and Table. 5, we have not observed obvious performance impact with different weather settings.

In order to make a fair model comparison between CIL++, MILE, and RIM, we have modified the scenario runner in order to handle the following two cases:

Intersection deadlock detection We observe that occasionally there are some intersection deadlocks, even though the dynamic density is not set to a high level. This could be caused by the random spawning and autopilot setting of the other vehicles in CARLA. To eliminate these cases for better comparison, we applied traffic detection. Once the traffic manager detects that some other vehicles stop within an intersection which is in 10 meters to the ego-vehicle for more than 90 seconds, the vehicles will be re-spawned to other points. As an illustration, we show an example of traffic deadlocks in Figure 3.

Global route re-planning As mentioned in our main paper, we applied real-time calibration on high-level navigation commands. When the ego-vehicle enters a lane out of the pre-planned global trajectory, a corrective command is forced, like *move-to-left-lane* or *move-to-right-lane* as soon as possible. However, in some cases, the ego-vehicle could not perform a lane changing since there might be some other vehicles on the target lane, which forces the ego vehicle to maintain on the driving lane. In this case, we apply the global route re-planning: once the traffic manager detects that the ego-vehicle deviates from the pre-planned route for more than 30 meters, a new route to the destination is computed, along with a new set of high-level commands to provide the ego-vehicle for driving.

5. Failure Case

We show one of our failure cases in Figure 4. The lane change command is given when the ego is close to the intersection while there is already another green vehicle on the right side lane. The ego agent could not make the right turn and change lane since it recognizes there is an obstacle. As the ego proceeds, the green vehicle also turns right and continues to occupy the space that is needed for ego to turn right. Eventually, when the ego arrives at the center of the intersection, the ego does not have enough space to turn right and stops.

	\uparrow SR(%)	\uparrow S.SR(%)	\uparrow Avg.RC(%)	\uparrow Avg.DS	\downarrow C.P	\downarrow C.V
Empty (numbers of vehicle/pedestrian: 0/0)						
RIM	99.0 \pm 0.0	93.7 \pm 0.6	99.0 \pm 0.0	97.4 \pm 0.2	0.0 \pm 0.0	0.0 \pm 0.0
CIL++	98.3 \pm 0.6	95.0 \pm 0.0	99.6 \pm 0.3	98.9 \pm 0.4	0.0 \pm 0.0	0.0 \pm 0.0
Expert	100.0 \pm 0.0	100.0 \pm 0.0	100.0 \pm 0.0	100.0 \pm 0.0	0.0 \pm 0.0	0.0 \pm 0.0
Regular (numbers of vehicle/pedestrian: 20/50)						
RIM	100.0 \pm 0.0	94.3 \pm 0.6	100.0 \pm 0.0	98.3 \pm 0.2	0.0 \pm 0.0	0.0 \pm 0.0
CIL++	99.3 \pm 0.6	99.3 \pm 0.6	99.8 \pm 0.2	99.8 \pm 0.2	0.0 \pm 0.0	0.0 \pm 0.0
Expert	100.0 \pm 0.0	100.0 \pm 0.0	100.0 \pm 0.0	100.0 \pm 0.0	0.0 \pm 0.0	0.0 \pm 0.0
Dense (numbers of vehicle/pedestrian: 100/250)						
RIM	91.5 \pm 3.5	76.0 \pm 7.1	97.6 \pm 2.1	90.9 \pm 3.7	5.1 \pm 7.2	23.4 \pm 16.1
CIL++	93.5 \pm 2.1	87.5 \pm 9.2	97.4 \pm 1.0	94.3 \pm 3.2	0.0 \pm 0.0	50.5 \pm 21.9
Expert	80.7 \pm 10.0	77.3 \pm 8.5	92.5 \pm 3.6	90.5 \pm 3.0	16.2 \pm 14.1	11.8 \pm 7.4

	\downarrow C.L	\downarrow T.L	\downarrow O.L	\downarrow R.Dev	\downarrow T.O	\downarrow A.B
Empty (numbers of vehicle/pedestrian: 0/0)						
RIM	0.0 \pm 0.0	18.5 \pm 2.4	0.0 \pm 0.0	0.0 \pm 0.0	0.0 \pm 0.0	73.4 \pm 0.0
CIL++	9.9 \pm 6.1	0.0 \pm 0.0	34.0 \pm 45.0	12.7 \pm 8.3	0.0 \pm 0.0	1.0 \pm 1.8
Expert	0.0 \pm 0.0	0.0 \pm 0.0	0.0 \pm 0.0	0.0 \pm 0.0	0.0 \pm 0.0	0.0 \pm 0.0
Regular (numbers of vehicle/pedestrian: 20/50)						
RIM	0.0 \pm 0.0	20.2 \pm 3.3	0.0 \pm 0.0	0.0 \pm 0.0	0.0 \pm 0.0	0.0 \pm 0.0
CIL++	0.0 \pm 0.0	0.0 \pm 0.0	0.0 \pm 0.0	0.0 \pm 0.0	0.0 \pm 0.0	2.1 \pm 1.8
Expert	0.0 \pm 0.0	0.0 \pm 0.0	0.0 \pm 0.0	0.0 \pm 0.0	0.0 \pm 0.0	0.0 \pm 0.0
Dense (numbers of vehicle/pedestrian: 100/250)						
RIM	0.0 \pm 0.0	79.9 \pm 33.6	0.0 \pm 0.0	0.0 \pm 0.0	14.1 \pm 0.3	36.8 \pm 52.0
CIL++	0.0 \pm 0.0	25.0 \pm 28.7	2.6 \pm 3.6	0.0 \pm 0.0	0.0 \pm 0.0	0.0 \pm 0.0
Expert	0.0 \pm 0.0	23.4 \pm 9.0	0.0 \pm 0.0	0.0 \pm 0.0	31.6 \pm 18.1	111.8 \pm 81.7

Table 4. *NoCrash* benchmark: Train Town (Town01) & Train Weather on 3 tasks: empty, regular, and dense. Mean and standard deviations are computed using three runs with different seeds. For \uparrow , the higher the better, while for \downarrow is the opposite. Due to page width constraints, we split the entire table into two sub-tables (Top: SR, S.SR, Avg.RC, Avg.DS, C.P, C.V; Bottom: C.L, T.L, O.L, R.Dev, T.O, A.B). All values are rounded to one decimal place.

	↑ SR(%)	↑ S.SR(%)	↑ Avg.RC(%)	↑ Avg.DS	↓ C.P	↓ C.V
Empty (numbers of vehicle/pedestrian: 0/0)						
RIM	100.0 ± 0.0	91.3 ± 1.2	100.0 ± 0.0	97.4 ± 0.3	0.0 ± 0.0	0.0 ± 0.0
CIL++	97.3 ± 3.1	94.0 ± 2.0	99.0 ± 0.9	98.2 ± 1.3	0.0 ± 0.0	0.0 ± 0.0
Expert	100.0 ± 0.0	100.0 ± 0.0	100.0 ± 0.0	100.0 ± 0.0	0.0 ± 0.0	0.0 ± 0.0
Regular (numbers of vehicle/pedestrian: 20/50)						
RIM	100.0 ± 0.0	88.7 ± 4.2	100.0 ± 0.0	96.6 ± 1.2	0.0 ± 0.0	0.0 ± 0.0
CIL++	98.0 ± 0.0	98.0 ± 0.0	98.9 ± 0.0	98.9 ± 0.0	0.0 ± 0.0	0.0 ± 0.0
Expert	100.0 ± 0.0	100.0 ± 0.0	100.0 ± 0.0	100.0 ± 0.0	0.0 ± 0.0	0.0 ± 0.0
Dense (numbers of vehicle/pedestrian: 100/250)						
RIM	94.7 ± 2.3	68.0 ± 7.2	98.4 ± 1.4	89.4 ± 3.5	0.0 ± 0.0	11.7 ± 17.0
CIL++	88.0 ± 4.0	83.3 ± 5.0	95.2 ± 3.1	91.9 ± 4.4	0.0 ± 0.0	12.8 ± 8.4
Expert	86.0 ± 9.2	84.7 ± 8.3	94.5 ± 3.6	93.2 ± 3.7	0.0 ± 0.0	6.7 ± 2.7

	↓ C.L	↓ T.L	↓ O.L	↓ R.Dev	↓ T.O	↓ A.B
Empty (numbers of vehicle/pedestrian: 0/0)						
RIM	0.0 ± 0.0	17.0 ± 4.6	0.0 ± 0.0	0.0 ± 0.0	0.0 ± 0.0	0.0 ± 0.0
CIL++	3.2 ± 5.5	0.0 ± 0.0	3.2 ± 5.5	5.2 ± 4.6	0.0 ± 0.0	11.3 ± 14.1
Expert	0.0 ± 0.0	0.0 ± 0.0	0.0 ± 0.0	0.0 ± 0.0	0.0 ± 0.0	0.0 ± 0.0
Regular (numbers of vehicle/pedestrian: 20/50)						
RIM	0.0 ± 0.0	26.4 ± 10.6	0.0 ± 0.0	0.0 ± 0.0	0.0 ± 0.0	0.0 ± 0.0
CIL++	0.0 ± 0.0	0.0 ± 0.0	0.0 ± 0.0	0.0 ± 0.0	0.0 ± 0.0	6.8 ± 0.0
Expert	0.0 ± 0.0	0.0 ± 0.0	0.0 ± 0.0	0.0 ± 0.0	0.0 ± 0.0	0.0 ± 0.0
Dense (numbers of vehicle/pedestrian: 100/250)						
RIM	0.0 ± 0.0	61.0 ± 19.5	0.0 ± 0.0	1.3 ± 2.3	4.3 ± 4.0	2.2 ± 3.9
CIL++	0.0 ± 0.0	8.3 ± 4.8	3.0 ± 5.2	0.0 ± 0.0	4.7 ± 5.2	1.0 ± 1.7
Expert	0.0 ± 0.0	1.7 ± 1.5	0.0 ± 0.0	0.0 ± 0.0	10.7 ± 9.7	30.5 ± 23.7

Table 5. *NoCrash* benchmark: Train Town (Town01) & New Weather on 3 tasks: empty, regular, dense. Mean and standard deviations are computed using three runs with different seeds. For ↑, the higher the better, while for ↓ is the opposite. Due to page width constraints, we split the entire table into two sub-tables (Top: SR, S.SR, Avg.RC, Avg.DS, C.P, C.V; Bottom: C.L, T.L, O.L, R.Dev, T.O, A.B). All values are rounded to one decimal place.

	\uparrow SR(%)	\uparrow S.SR(%)	\uparrow Avg.RC(%)	\uparrow Avg.DS	\downarrow C.P	\downarrow C.V
Empty (numbers of vehicle/pedestrian: 0/0)						
RIM	84.7 ± 1.2	67.3 ± 1.5	93.0 ± 1.0	85.3 ± 0.6	0.0 ± 0.0	0.0 ± 0.0
CIL++	100.0 ± 0.0	100.0 ± 0.0	100.0 ± 0.0	100.0 ± 0.0	0.0 ± 0.0	0.0 ± 0.0
Expert	100.0 ± 0.0	100.0 ± 0.0	100.0 ± 0.0	100.0 ± 0.0	0.0 ± 0.0	0.0 ± 0.0
Regular (numbers of vehicle/pedestrian: 15/50)						
RIM	82.7 ± 2.1	71.3 ± 4.0	92.7 ± 0.8	86.2 ± 1.5	0.0 ± 0.0	208.8 ± 261.5
CIL++	93.7 ± 6.1	93.0 ± 6.2	97.3 ± 2.7	95.7 ± 4.2	0.0 ± 0.0	111.7 ± 134.2
Expert	95.3 ± 1.2	95.0 ± 1.0	99.8 ± 0.2	99.6 ± 0.3	0.0 ± 0.0	2.9 ± 5.0
Busy (numbers of vehicle/pedestrian: 70/70)						
RIM	66.0 ± 1.7	50.7 ± 2.1	86.4 ± 1.9	76.4 ± 1.9	19.2 ± 33.3	505.8 ± 260.9
CIL++	73.7 ± 11.6	69.3 ± 11.7	89.0 ± 6.2	82.8 ± 7.1	0.0 ± 0.0	361.8 ± 319.1
Expert	84.7 ± 8.1	81.3 ± 7.6	93.8 ± 2.1	91.4 ± 1.9	0.0 ± 0.0	273.6 ± 297.8

	\downarrow C.L	\downarrow T.L	\downarrow O.L	\downarrow R.Dev	\downarrow T.O	\downarrow A.B
Empty (numbers of vehicle/pedestrian: 0/0)						
RIM	684.0 ± 44.4	123.0 ± 13.5	683.6 ± 50.5	20.1 ± 9.8	0.0 ± 0.0	28.4 ± 49.1
CIL++	0.0 ± 0.0	0.0 ± 0.0	0.0 ± 0.0	0.0 ± 0.0	0.0 ± 0.0	0.0 ± 0.0
Expert	0.0 ± 0.0	0.0 ± 0.0	0.0 ± 0.0	0.0 ± 0.0	0.0 ± 0.0	0.0 ± 0.0
Regular (numbers of vehicle/pedestrian: 15/50)						
RIM	$510. \pm 183.4$	93.9 ± 53.7	547.2 ± 174.7	20.3 ± 30.7	9.3 ± 8.1	0.0 ± 0.0
CIL++	7.0 ± 12.2	5.3 ± 4.7	3.5 ± 6.1	0.0 ± 0.0	0.0 ± 0.0	3.5 ± 6.1
Expert	0.0 ± 0.0	2.4 ± 4.2	0.0 ± 0.0	0.0 ± 0.0	26.4 ± 4.9	0.0 ± 0.0
Busy (numbers of vehicle/pedestrian: 70/70)						
RIM	390.5 ± 223.3	274.2 ± 46.2	470.7 ± 245.3	7.8 ± 9.3	182.6 ± 17.7	19.2 ± 33.3
CIL++	0.0 ± 0.0	131.5 ± 39.2	1.9 ± 3.3	0.0 ± 0.0	80.4 ± 27.5	0.0 ± 0.0
Expert	0.0 ± 0.0	77.1 ± 29.1	0.0 ± 0.0	0.0 ± 0.0	217.7 ± 122.9	0.0 ± 0.0

Table 6. *NoCrash* benchmark: New Town (Town02) & Train Weather on 3 tasks: empty, regular, busy. Mean and standard deviations are computed using three runs with different seeds. For \uparrow , the higher the better, while for \downarrow is the opposite. Due to page width constraints, we split the entire table into two sub-tables (Top: SR, S.SR, Avg.RC, Avg.DS, C.P, C.V; Bottom: C.L, T.L, O.L, R.Dev, T.O, A.B). All values are rounded to one decimal place.

	↑ SR(%)	↑ S.SR(%)	↑ Avg.RC(%)	↑ Avg.DS	↓ C.P	↓ C.V
Empty (numbers of vehicle/pedestrian: 0/0)						
RIM	100.0 ± 0.0	85.3 ± 1.2	100.0 ± 0.0	95.6 ± 0.3	0.0 ± 0.0	0.0 ± 0.0
CIL++	100.0 ± 0.0	100.0 ± 0.0	100.0 ± 0.0	100.0 ± 0.0	0.0 ± 0.0	0.0 ± 0.0
Expert	100.0 ± 0.0	100.0 ± 0.0	100.0 ± 0.0	100.0 ± 0.0	0.0 ± 0.0	0.0 ± 0.0
Regular (numbers of vehicle/pedestrian: 15/50)						
RIM	96.7 ± 2.3	86.0 ± 7.2	100.0 ± 0.0	95.3 ± 1.6	0.0 ± 0.0	5.0 ± 6.2
CIL++	98.7 ± 2.3	96.7 ± 3.1	99.5 ± 0.8	98.9 ± 1.0	0.0 ± 0.0	5.0 ± 8.7
Expert	100.0 ± 0.0	96.7 ± 1.2	100.0 ± 0.0	99.0 ± 0.3	0.0 ± 0.0	0.0 ± 0.0
Busy (numbers of vehicle/pedestrian: 70/70)						
RIM	81.3 ± 5.0	68.0 ± 7.2	95.0 ± 1.0	89.4 ± 2.8	0.0 ± 0.0	63.4 ± 52.7
CIL++	82.7 ± 7.6	76.7 ± 7.6	92.4 ± 3.5	88.0 ± 3.2	0.0 ± 0.0	44.8 ± 21.5
Expert	84.0 ± 2.0	82.0 ± 2.0	95.9 ± 0.2	94.5 ± 0.2	0.0 ± 0.0	36.5 ± 14.1

	↓ C.L	↓ T.L	↓ O.L	↓ R.Dev	↓ T.O	↓ A.B
Empty (numbers of vehicle/pedestrian: 0/0)						
RIM	0.0 ± 0.0	65.6 ± 5.2	0.0 ± 0.0	0.0 ± 0.0	0.0 ± 0.0	0.0 ± 0.0
CIL++	0.0 ± 0.0	0.0 ± 0.0	0.0 ± 0.0	0.0 ± 0.0	0.0 ± 0.0	0.0 ± 0.0
Expert	0.0 ± 0.0	0.0 ± 0.0	0.0 ± 0.0	0.0 ± 0.0	0.0 ± 0.0	0.0 ± 0.0
Regular (numbers of vehicle/pedestrian: 15/50)						
RIM	0.0 ± 0.0	65.9 ± 53.6	0.0 ± 0.0	0.0 ± 0.0	0.0 ± 0.0	0.0 ± 0.0
CIL++	0.0 ± 0.0	6.7 ± 7.9	0.0 ± 0.0	0.0 ± 0.0	0.0 ± 0.0	0.0 ± 0.0
Expert	0.0 ± 0.0	12.7 ± 4.6	0.0 ± 0.0	0.0 ± 0.0	0.0 ± 0.0	0.0 ± 0.0
Busy (numbers of vehicle/pedestrian: 70/70)						
RIM	0.0 ± 0.0	85.7 ± 40.0	5.9 ± 10.2	0.0 ± 0.0	70.6 ± 45.7	0.0 ± 0.0
CIL++	0.0 ± 0.0	48.8 ± 32.7	3.6 ± 6.2	0.0 ± 0.0	28.6 ± 42.3	0.0 ± 0.0
Expert	0.0 ± 0.0	17.5 ± 13.0	0.0 ± 0.0	0.0 ± 0.0	107.6 ± 16.0	0.0 ± 0.0

Table 7. *NoCrash* benchmark: New Town (Town02) & New Weather on 3 tasks: empty, regular, busy. Mean and standard deviations are computed using three runs with different seeds. For ↑, the higher the better, while for ↓ is the opposite. Due to page width constraints, we split the entire table into two sub-tables (Top: SR, S.SR, Avg.RC, Avg.DS, C.P, C.V; Bottom: C.L, T.L, O.L, R.Dev, T.O, A.B). All values are rounded to one decimal place.

	\uparrow Avg.RC(%)	\uparrow Avg.DS	\downarrow C.P	\downarrow C.V	\downarrow C.L
Numbers of vehicle/pedestrian: 70/70					
RIM	97.4 ± 1.3	70.6 ± 5.2	0.0 ± 0.0	9.1 ± 0.5	4.7 ± 7.1
MILE	84.9 ± 3.9	62.1 ± 3.4	0.0 ± 0.0	28.2 ± 16.3	8.6 ± 6.3
CIL++	87.7 ± 0.9	59.3 ± 1.0	4.1 ± 7.1	13.9 ± 1.7	9.9 ± 4.2
Expert	97.4 ± 0.4	85.0 ± 3.6	0.0 ± 0.0	8.1 ± 1.2	0.0 ± 0.0

	\downarrow T.L	\downarrow O.L	\downarrow R.Dev	\downarrow T.O	\downarrow A.B
Numbers of vehicle/pedestrian: 70/70					
RIM	18.4 ± 4.0	14.3 ± 1.4	1.3 ± 0.4	0.0 ± 0.0	5.8 ± 6.2
MILE	9.9 ± 3.6	26.0 ± 12.8	0.3 ± 0.5	0.0 ± 0.0	27.8 ± 13.1
CIL++	8.7 ± 7.5	25.6 ± 5.1	27.1 ± 14.3	0.0 ± 0.0	21.7 ± 3.9
Expert	1.7 ± 0.9	0.0 ± 0.0	0.0 ± 0.0	0.0 ± 0.0	2.3 ± 0.6

Table 8. *Multi-lane town* experiments: Train Town (Town03) & Train Weather. Mean and standard deviations are computed using three runs with different seeds. For \uparrow , the higher the better, while for \downarrow is the opposite. Due to page width constraints, we split the entire table into two sub-tables (Top: Avg.RC, Avg.DS, C.P, C.V, C.L; Bottom: T.L, O.L, R.Dev, T.O, A.B). All values are rounded to one decimal place.

	\uparrow Avg.RC(%)	\uparrow Avg.DS	\downarrow C.P	\downarrow C.V	\downarrow C.L
Numbers of vehicle/pedestrian: 120/120					
RIM	92.0 ± 3.1	50.6 ± 7.9	0.0 ± 0.0	7.5 ± 1.3	4.3 ± 1.6
MILE	98.2 ± 2.2	72.7 ± 2.9	0.0 ± 0.0	6.0 ± 3.6	0.0 ± 0.0
CIL++	97.9 ± 1.7	67.8 ± 2.7	0.0 ± 0.0	6.0 ± 0.5	3.8 ± 0.7
Expert	99.5 ± 0.8	89.4 ± 1.7	0.0 ± 0.0	3.2 ± 1.1	0.0 ± 0.0

	\downarrow T.L	\downarrow O.L	\downarrow R.Dev	\downarrow T.O	\downarrow A.B
Numbers of vehicle/pedestrian: 120/120					
RIM	26.0 ± 8.9	5.4 ± 2.7	3.0 ± 3.2	0.0 ± 0.0	73.5 ± 120.3
MILE	3.6 ± 3.8	3.5 ± 1.5	0.0 ± 0.0	0.0 ± 0.0	1.9 ± 2.0
CIL++	5.8 ± 5.1	6.1 ± 2.2	9.4 ± 3.6	0.0 ± 0.0	1.7 ± 1.3
Expert	1.3 ± 0.4	0.0 ± 0.0	0.0 ± 0.0	0.0 ± 0.0	0.5 ± 0.8

Table 9. *Multi-lane town* experiments: New Town (Town05) & New Weather. Mean and standard deviations are computed using three runs with different seeds. For \uparrow , the higher the better, while for \downarrow is the opposite. Due to page width constraints, we split the entire table into two sub-tables (Top: Avg.RC, Avg.DS, C.P, C.V, C.L; Bottom: T.L, O.L, R.Dev, T.O, A.B). All values are rounded to one decimal place.



(a) A typical urban scene in Town05 in CARLA 0.9.11, with the ClearNoon weather setting.



(b) The same scene as (a) with the same ClearNoon weather setting, on CARLA 0.9.13. Note the difference in shadow length, clouds, and general lighting compared to CARLA 0.9.11.

Figure 2. ClearNoon weather condition in two versions of CARLA. Please refer to Table 10 for the specific parameters each version uses.

	CARLA 0.9.11	CARLA 0.9.13
cloudiness	15.0000	5.0000
precipitation	0.0000	0.0000
precipitation_deposits	0.0000	0.0000
wind_intensity	0.3500	10.0000
sun_azimuth_angle	0.0000	-1.0000
sun_altitude_angle	75.0000	45.0000
fog_density	0.0000	2.0000
fog_distance	0.0000	0.7500
fog_falloff	0.0000	0.1000
wetness	0.0000	0.0000
scattering_intensity	N/A	1.0000
mie_scattering_scale	N/A	0.0300
rayleigh_scattering_scale	N/A	0.0331

Table 10. We take ClearNoon as an example to show weather settings differences between different versions of CARLA. Note that the last three parameters, namely `scattering_intensity`, `mie_scattering_scale`, and `rayleigh_scattering_scale` are available only since CARLA 0.9.12. For the full explanation and usage of each variable, please refer to the CARLA documentation [here](#).



Figure 3. An example of traffic deadlocks in Town05 that could lead to a timeout in route completion.

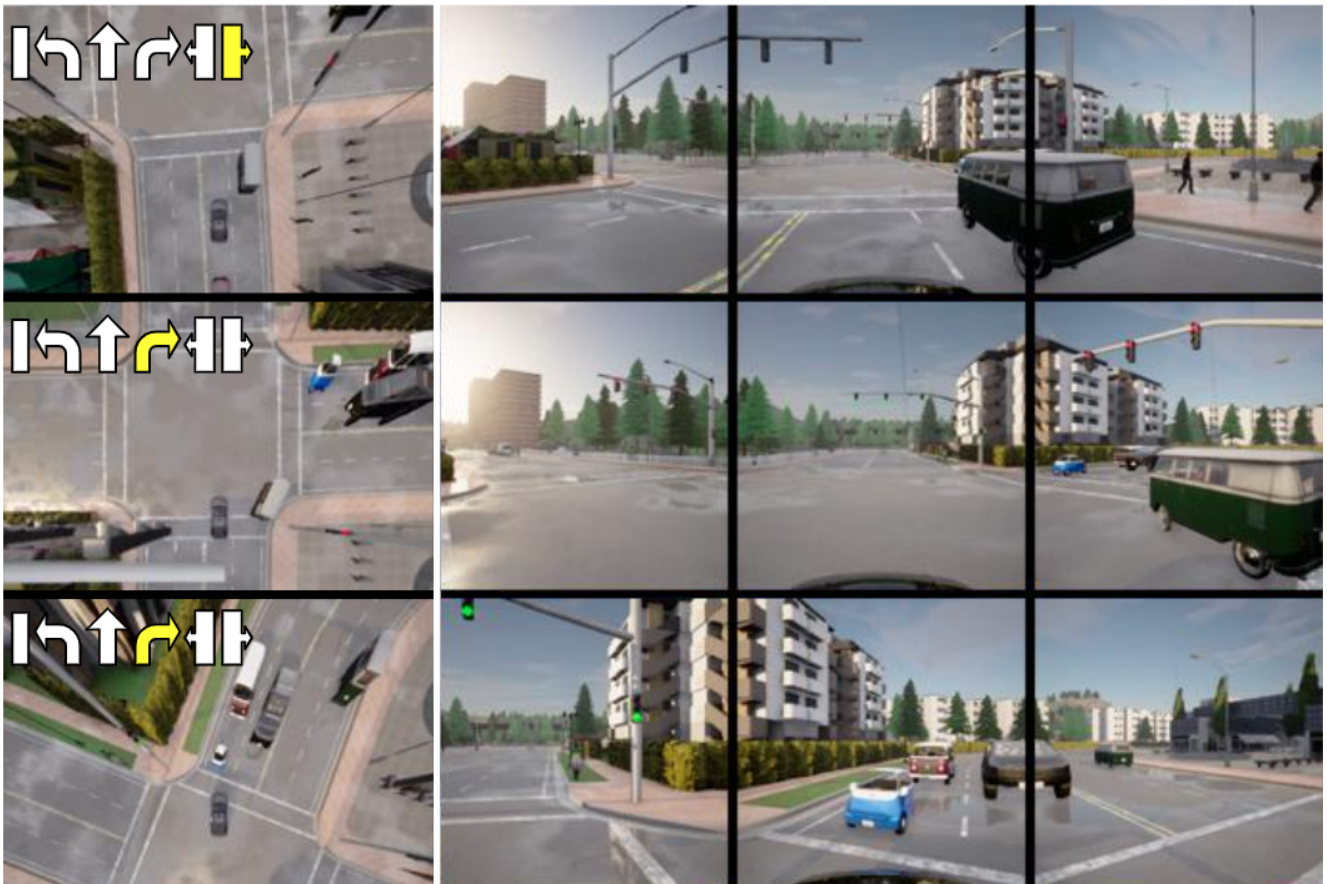


Figure 4. One failure case of CIL++ at intersection caused by a dilemma situation: the *move-to-right-lane* navigation command is provided around the intersection, while there is another vehicle blocking the target lane. As the ego proceeds a right turn, the other vehicle also turns right and occupies the space required for the ego-vehicle to make right turn, which leads to a failure.

References

- [1] Jimmy Lei Ba, Jamie Ryan Kiros, and Geoffrey E Hinton. Layer normalization, 2016. 4
- [2] Mayank Bansal, Alex Krizhevsky, and Abhijit S. Ogale. ChauffeurNet: Learning to drive by imitating the best and synthesizing the worst. In *Robotics: Science and Systems (RSS)*, 2019.
- [3] Mariusz Bojarski, Davide Del Testa, Daniel Dworakowski, Bernhard Firner, Beat Flepp, Praseoon Goyal, Lawrence D. Jackel, Mathew Monfort, Urs Muller, Jiakai Zhang, Xin Zhang, Jake Zhao, and Karol Zieba. End to end learning for self-driving cars. arXiv:1712.00409, 2016.
- [4] M. Bojarski, P. Yeres, A. Choromanska, K. Choromanski, B. Firner, L. Jackel, and U. Muller. Explaining how a deep neural network trained with end-to-end learning steers a car. arXiv:1704.07911, 2017.
- [5] Dian Chen and Philipp Krähenbühl. Learning from all vehicles. In *Int. Conf. on Computer Vision and Pattern Recognition (CVPR)*, 2022.
- [6] Dian Chen, Brady Zhou, Vladlen Koltun, and Philipp Krähenbühl. Learning by cheating. In *Conf. on Robot Learning (CoRL)*, 2019.
- [7] Kashyap Chitta, Aditya Prakash, and Andreas Geiger. NEAT: Neural attention fields for end-to-end autonomous driving. In *Inter. Conf. on Computer Vision (ICCV)*, 2021.
- [8] Felipe Codevilla, Matthias Müller, Antonio M. López, Vladlen Koltun, and Alexey Dosovitskiy. End-to-end driving via conditional imitation learning. In *Inter. Conf. on Robotics and Automation (ICRA)*, 2018.
- [9] Felipe Codevilla, Edgar Santana, Antonio M. López, and Adrien Gaidon. Exploring the limitations of behavior cloning for autonomous driving. In *Inter. Conf. on Computer Vision (ICCV)*, 2019.
- [10] Pim De Haan, Dinesh Jayaraman, and Sergey Levine. Causal confusion in imitation learning. In *Neural Information Processing Systems (NeurIPS)*, 2019.
- [11] Jia Deng, Wei Dong, Richard Socher, Li-Jia Li, Kai Li, and Li Fei-Fei. ImageNet: A large-scale hierarchical image database. In *Int. Conf. on Computer Vision and Pattern Recognition (CVPR)*, 2009.
- [12] Alexey Dosovitskiy, Lucas Beyer, Alexander Kolesnikov, Dirk Weissenborn, Xiaohua Zhai, Thomas Unterthiner, Mostafa Dehghani, Matthias Minderer, Georg Heigold, Sylvain Gelly, Jakob Uszkoreit, and Neil Houlsby. An image is worth 16x16 words: Transformers for image recognition at scale. In *Inter. Conf. on Learning Representation (ICLR)*, 2021.
- [13] Alexey Dosovitskiy, German Ros, Felipe Codevilla, Antonio López, and Vladlen Koltun. CARLA: An open urban driving simulator. In *Conf. on Robot Learning (CoRL)*, 2017. 1
- [14] Sorin Grigorescu, Bogdan Tranea, Tiberiu Cocias, and Gigel Macesanu. A survey of deep learning techniques for autonomous driving. *Journal of Field Robotics*, 37(3):362–386, 2020.
- [15] Kaiming He, Xiangyu Zhang, Shaoqing Ren, and Jian Sun. Deep residual learning for image recognition. In *Int. Conf. on Computer Vision and Pattern Recognition (CVPR)*, 2016.
- [16] Anthony Hu, Gianluca Corrado, Nicolas Griffiths, Zak Murez, Corina Gurau, Hudson Yeo, Alex Kendall, Roberto Cipolla, and Jamie Shotton. Model-based imitation learning for urban driving. In *Neural Information Processing Systems (NeurIPS)*, 2022. 1
- [17] Diederik P Kingma and Jimmy Ba. Adam: A method for stochastic optimization. In *Inter. Conf. on Learning Representation (ICLR)*, 2015.
- [18] Yann LeCun, Urs Muller, Jan Ben, Eric Cosatto, and Beat Flepp. Off-road obstacle avoidance through end-to-end learning. In *Neural Information Processing Systems (NIPS)*, 2005.
- [19] Xiaodan Liang, Tairui Wang, Luona Yang, and Eric Xing. CIRL: Controllable imitative reinforcement learning for vision-based self-driving. In *European Conf. on Computer Vision (ECCV)*, 2018.
- [20] Matthias Mueller, Alexey Dosovitskiy, Bernard Ghanem, and Vladlen Koltun. Driving policy transfer via modularity and abstraction. In *Conf. on Robot Learning (CoRL)*, 2018.
- [21] Yunpeng Pan, Ching-An Cheng, Kamil Saigol, Keuntaek Lee, Xinyan Yan, Evangelos A Theodorou, and Byron Boots. Agile autonomous driving using end-to-end deep imitation learning. In *Robotics: Science and Systems (RSS)*, 2018.
- [22] Dean Pomerleau. ALVINN: An autonomous land vehicle in a neural network. In *Neural Information Processing Systems (NIPS)*, 1989.
- [23] Aditya Prakash, Kashyap Chitta, and Andreas Geiger. Multi-modal fusion transformer for end-to-end autonomous driving. In *Int. Conf. on Computer Vision and Pattern Recognition (CVPR)*, 2021.
- [24] Ramprasaath R Selvaraju, Michael Cogswell, Abhishek Das, Ramakrishna Vedantam, Devi Parikh, and Dhruv Batra. Grad-cam: Visual explanations from deep networks via gradient-based localization. In *Inter. Conf. on Computer Vision (ICCV)*, 2017.

- [25] Hao Shao, Letian Wang, Ruobing Chen, Hongsheng Li, and Yu Liu. InterFuser: Safety-enhanced autonomous driving using interpretable sensor fusion transformer. In *Conf. on Robot Learning (CoRL)*, 2022.
- [26] Jonathan Spencer, Sanjiban Choudhury, Arun Venkatraman, Brian Ziebart, and J Andrew Bagnell. Feedback in imitation learning: The three regimes of covariate shift. arXiv:2102.02872, 2021.
- [27] Ardi Tampuu, Tambet Matiisen, Maksym Semikin, Dmytro Fishman, and Naveed Muhammad. A survey of end-to-end driving: Architectures and training methods. *IEEE Trans. on Neural Networks and Learning Systems*, 33(4):1364–1384, 2022.
- [28] Learning to drive from simulation without real world labels. Bewley, alex and rigley, jessica and liu, yuxuan and hawke, jeffrey and shen, richard and lam, vinh-dieu and kendall, alex. In *Inter. Conf. on Robotics and Automation (ICRA)*, 2019.
- [29] Marin Toromanoff, Emilie Wirbel, and Fabien Moutarde. End-to-end model-free reinforcement learning for urban driving using implicit affordances. In *Int. Conf. on Computer Vision and Pattern Recognition (CVPR)*, 2020.
- [30] Ashish Vaswani, Noam Shazeer, Niki Parmar, Jakob Uszkoreit, Llion Jones, Aidan N Gomez, Łukasz Kaiser, and Illia Polosukhin. Attention is all you need. In *Neural Information Processing Systems (NeurIPS)*, 2017.
- [31] Penghao Wu, Xiaosong Jia, Li Chen, Junchi Yan, Hongyang Li, and Yu Qiao. Trajectory-guided control prediction for end-to-end autonomous driving: A simple yet strong baseline. In *Neural Information Processing Systems (NeurIPS)*, 2022.
- [32] Yi Xiao, Felipe Codevilla, Akhil Gurram, Onay Urfalioglu, and Antonio M López. Multimodal end-to-end autonomous driving. *IEEE Trans. on Intelligent Transportation Systems*, 23(1):537–547, 2020.
- [33] Ekim Yurtsever, Jacob Lambert, Alexander Carballo, and Kazuya Takeda. A survey of autonomous driving: Common practices and emerging technologies. *IEEE Access*, 8:58443–58469, 2020.
- [34] Zhejun Zhang, Alexander Liniger, Dengxin Dai, Fisher Yu, and Luc Van Gool. End-to-end urban driving by imitating a reinforcement learning coach. In *Inter. Conf. on Computer Vision (ICCV)*, 2021. [1](#), [2](#)